

serum (Omega Scientific) in RPMI 1640 with 10 mM HEPES buffer, 2 mM l-glutamine, 100 U ml<sup>-1</sup> penicillin and 100 µg ml<sup>-1</sup> streptomycin (all from Cambrex BioScience). T-cell clones were expanded with IL-2, assayed on day 9 or 10 post-stimulation and re-stimulated as previously described<sup>11</sup>.

Antigen reactivity was examined using irradiated (5,000 rads) Priess EBV-transformed B cells (homozygous for DRB1\*0401) or QBL B cells (homozygous for DRB1\*0301) pulsed with peptide (250 µM for Fig. 1a) in the presence or absence of antibody (10 µg ml<sup>-1</sup> anti-DR LB3.1 and anti-DQ IVD12) for 2 h, washed and plated in triplicate at 50,000 cells per well with equal numbers of T-cell clones. Each T-cell clone was also plated onto plate-bound anti-CD3 antibody (OKT3; 0.05 µg per well) to assess the viability of each clone in each experiment. After 48 h, 20 U ml<sup>-1</sup> IL-2 was added to each well. Supernatants were collected after a further 24 h for measurement by cytokine ELISA (BD PharMingen). For testing of T-cell clones from the type 2 diabetic subject NCI, irradiated, autologous pancreatic draining lymph node cells were pulsed with pools of peptides (each at 250 µM) for 2 h, washed and plated at 120,000 cells per well with 50,000 T cells. The remainder of the assay was as described above.

## Sequencing of T-cell receptors

RNAs were isolated using the standard RNAzol method (Tel-Test). Complementary DNAs were synthesized using Superscript Reverse Transcriptase (Gibco) and oligo dT as the primer for reverse transcription. PCR primers for both V<sub>α</sub> and V<sub>β</sub> families were designed and grouped according to refs 31 and 32. PCR products were purified from agarose gel and subjected to DNA sequencing (Brigham & Women's Hospital Sequencing Facility). The V<sub>α</sub> and V<sub>β</sub> sequences obtained were aligned against the ImmunoGeneTics (IMGT) database.

Received 14 March; accepted 11 April 2005; doi:10.1038/nature03625.

- Atkinson, M. A. & Maclaren, N. K. The pathogenesis of insulin-dependent diabetes mellitus. *N. Engl. J. Med.* **331**, 1428–1436 (1994).
- Eisenbarth, G. S. Type I diabetes mellitus: a chronic autoimmune disease. *N. Engl. J. Med.* **314**, 1360–1368 (1986).
- Hoglund, P. et al. Initiation of autoimmune diabetes by developmentally regulated presentation of islet cell antigens in the pancreatic lymph nodes. *J. Exp. Med.* **189**, 331–339 (1999).
- Thomson, G. et al. Genetic heterogeneity, modes of inheritance, and risk estimates for a joint study of Caucasians with insulin-dependent diabetes mellitus. *Am. J. Hum. Genet.* **43**, 799–816 (1988).
- Katz, J. D., Wang, B., Haskins, K., Benoist, C. & Mathis, D. Following a diabetogenic T cell from genesis through pathogenesis. *Cell* **74**, 1089–1100 (1993).
- Acha-Orbea, H. & McDevitt, H. O. The role of class II molecules in development of insulin-dependent diabetes mellitus in mice, rats and humans. *Curr. Top. Microbiol. Immunol.* **156**, 103–119 (1990).
- Haskins, K., Portas, M., Bergman, B., Lafferty, K. & Bradley, B. Pancreatic islet-specific T-cell clones from nonobese diabetic mice. *Proc. Natl Acad. Sci. USA* **86**, 8000–8004 (1989).
- Wegmann, D. R., Norbury-Glaser, M. & Daniel, D. Insulin-specific T cells are a predominant component of islet infiltrates in pre-diabetic NOD mice. *Eur. J. Immunol.* **24**, 1853–1857 (1994).
- Londei, M. et al. Persistence of collagen type II-specific T-cell clones in the synovial membrane of a patient with rheumatoid arthritis. *Proc. Natl Acad. Sci. USA* **86**, 636–640 (1989).
- Dayan, C. M. et al. Autoantigen recognition by thyroid-infiltrating T cells in Graves disease. *Proc. Natl Acad. Sci. USA* **88**, 7415–7419 (1991).
- Hafner, D. A. et al. Oligoclonal T-lymphocytes in the cerebrospinal fluid of patients with inflammatory central nervous system diseases. *J. Exp. Med.* **167**, 1625–1644 (1988).
- Roep, B. O. T-cell responses to autoantigens in IDDM. *Diabetes* **45**, 1147–1156 (1996).
- Wong, F. S. et al. Identification of an MHC class II-restricted autoantigen in type 1 diabetes by screening an organ-specific cDNA library. *Nature Med.* **5**, 1026–1031 (1999).
- Todd, J. A., Bell, J. I. & McDevitt, H. O. HLA antigens and insulin-dependent diabetes. *Nature* **333**, 710 (1988).
- Schlott, N. C. et al. Comparison of cytokine ELISpot assay formats for the detection of islet antigen autoreactive T cells. Report of the third immunology of diabetes society T-cell workshop. *J. Autoimmun.* **21**, 365–376 (2003).
- Peakman, M. et al. Characterization of preparations of GAD65, proinsulin, and the islet tyrosine phosphatase IA-2 for use in detection of autoreactive T-cells in type 1 diabetes: report of phase II of the Second International Immunology of Diabetes Society Workshop for Standardization of T-cell assays in type 1 diabetes. *Diabetes* **50**, 1749–1754 (2001).
- Eisenbarth, G. S. et al. Insulin autoimmunity: prediction/precipitation/prevention type 1A diabetes. *Autoimmun. Rev.* **1**, 139–145 (2002).
- Harrison, L. C. et al. Islet-reactive T cells are a marker of preclinical insulin-dependent diabetes. *J. Clin. Invest.* **89**, 1161–1165 (1992).
- Astill, T. P., Ellis, R. J., Arif, S., Tree, T. I. M. & Peakman, M. Promiscuous binding of proinsulin peptides to Type 1 diabetes-permissive and -protective HLA class II molecules. *Diabetologia* **46**, 496–503 (2003).
- Endl, J. et al. Identification of naturally processed T cell epitopes from glutamic acid decarboxylase presented in the context of HLA-DR alleles by T lymphocytes of recent onset IDDM patients. *J. Clin. Invest.* **15**, 2405–2415 (1997).
- Mycko, M. P. et al. Cross-reactive TCR responses to self antigens presented by different MHC class II molecules. *J. Immunol.* **173**, 1689–1698 (2004).
- Tian, J., Lehmann, P. & Kaufman, D. Determinant spreading of T helper cell 2 (Th2) responses to pancreatic islet autoantigens. *J. Exp. Med.* **186**, 2039–2043 (1997).
- Nakano, N., Kikutani, H., Nishimoto, H. & Kishimoto, T. T cell receptor V gene usage of islet β cell-reactive T cells is not restricted in non-obese diabetic mice. *J. Exp. Med.* **173**, 1091–1097 (1991).
- Miyazaki, A. et al. Predominance of T lymphocytes in pancreatic islets and spleen of pre-diabetic non-obese diabetic (NOD) mice: a longitudinal study. *Clin. Exp. Immunol.* **60**, 622–630 (1985).
- Candea, S., Katz, J., Benoist, C., Mathis, D. & Haskins, K. Islet-specific T-cell clones from nonobese diabetic mice express heterogeneous T-cell receptors. *Proc. Natl Acad. Sci. USA* **88**, 6167–6170 (1991).
- Baker, F., Lee, M., Chien, Y.-h. & Davis, M. Restricted islet-cell reactive T cell repertoire of early pancreatic islet infiltrates in NOD mice. *Proc. Natl Acad. Sci. USA* **99**, 9374–9379 (2002).
- Sibley, R. K., Sutherland, D. E., Goetz, F. & Michael, A. F. Recurrent diabetes mellitus in the pancreas

- iso- and allograft. A light and electron microscopic and immunohistochemical analysis of four cases. *Lab. Invest.* **53**, 132–144 (1985).
- Jaekel, E., Lipes, M. A. & von Boehmer, H. Recessive tolerance to preproinsulin 2 reduces but does not abolish type 1 diabetes. *Nature Immunol.* **5**, 1028–1035 (2004).
- Nakayama, M. et al. Prime role for an insulin epitope in the development of type 1 diabetes in NOD mice. *Nature* doi:10.1038/nature03523 (this issue).
- Yoon, J. W. et al. Control of autoimmune diabetes in NOD mice by GAD expression or suppression in beta cells. *Science* **284**, 1183–1187 (1999).
- Han, M. et al. Invariant or highly conserved TCR α are expressed on double-negative (CD3<sup>+</sup>CD4<sup>-</sup>CD8<sup>-</sup>) and CD8<sup>+</sup> T cells. *J. Immunol.* **163**, 301–311 (1999).
- Akatsuka, Y., Martin, E., Madonik, A., Barsoukov, A. & Hansen, J. Rapid screening of T-cell receptor (TCR) variable gene usage by multiplex PCR: application for assessment of clonal composition. *Tissue Antigens* **53**, 122–134 (1999).

Supplementary Information accompanies the paper on [www.nature.com/nature](http://www.nature.com/nature).

**Acknowledgements** We thank V. Kuchroo and G. Fathman for critical reading of the manuscript. We thank G. Nepom for B cell lines, and R. Neal Smith and N. Kirchof for expert immunohistochemical and histological tissue staining. These studies were supported by grants to D.A.H. (NIH), to Y.C. (JDRFI Fellowship), to L.B. (NMSS Fellowship) and to S.C.K. (Boston Area Diabetes Endocrinology Research Center). D.A.H. is a recipient of the NIH Javits Investigator Award.

**Competing interests statement** The authors declare that they have no competing financial interests.

**Correspondence** and requests for materials should be addressed to D.A.H. (dhafler@rics.bwh.harvard.edu).

## Enhancement of cellular memory by reducing stochastic transitions

Murat Acar, Attila Becskei & Alexander van Oudenaarden

Department of Physics, Massachusetts Institute of Technology, Cambridge, Massachusetts 02139, USA

On induction of cell differentiation, distinct cell phenotypes are encoded by complex genetic networks<sup>1–3</sup>. These networks can prevent the reversion of established phenotypes even in the presence of significant fluctuations. Here we explore the key parameters that determine the stability of cellular memory by using the yeast galactose-signalling network as a model system. This network contains multiple nested feedback loops. Of the two positive feedback loops, only the loop mediated by the cytoplasmic signal transducer Gal3p is able to generate two stable expression states with a persistent memory of previous galactose consumption states. The parallel loop mediated by the galactose transporter Gal2p only increases the expression difference between the two states. A negative feedback through the inhibitor Gal80p reduces the strength of the core positive feedback. Despite this, a constitutive increase in the Gal80p concentration tunes the system from having destabilized memory to having persistent memory. A model reveals that fluctuations are trapped more efficiently at higher Gal80p concentrations. Indeed, the rate at which single cells randomly switch back and forth between expression states was reduced. These observations provide a quantitative understanding of the stability and reversibility of cellular differentiation states.

Complex gene and protein networks store cellular memory by creating two or many discrete, stable states of network activity<sup>4–6</sup>. The generation of bistability by simple feedback loops in synthetic circuits is well understood<sup>7–10</sup>. However, naturally occurring networks, in particular in eukaryotic organisms, possess a complex organization of multiple nested feedback loops, making an analysis of system dynamics disproportionately more complicated<sup>11,12</sup>. These networks are exemplified by the galactose signalling pathway

in the yeast *Saccharomyces cerevisiae*. Despite extensive data on its molecular interactions, a prediction of its dynamical system behaviour a priori is challenging<sup>13,14</sup>. The galactose signal propagates through a four-stage signalling cascade. At the uppermost stage is Gal2p, which imports extracellular galactose into the cell. Subsequently, intracellular galactose binds to and activates Gal3p (refs 15, 16). At the third stage of this cascade, the activated Gal3p binds to and sequesters Gal80p in the cytoplasm, depleting Gal80p from the nucleus<sup>17</sup>. The transcriptional activator Gal4p, which is constitutively bound to promoters of the *GAL* genes<sup>18</sup>, is then released from the inhibitory action of Gal80p and activates expression of genes at the output of the cascade, including *GAL1*, *GAL2*, *GAL3* and *GAL80*. Because an increase in Gal2p and Gal3p concentration results in enhanced transcriptional activity, these proteins close two positive feedback loops. The opposite holds for Gal80p, which is part of a negative feedback loop. To read out the Gal4p activity in single yeast cells we monitored the expression of yellow fluorescent protein (YFP) driven by the *GAL1* promoter (Fig. 1).

Because the GAL regulatory network contains two positive feedback loops, this network has the potential for exhibiting multistability. A convenient experimental way to probe for multistability is to subject the network to different initial conditions and explore whether the network gets locked in different stable expression states. We therefore grew wild-type cells for 12 h either in the absence of galactose ('raffinose history') or in the presence of 2% galactose ('galactose history') and subsequently for a further 27 h at various concentrations of galactose. Raffinose was chosen as a neutral sugar because it neither activates nor represses the galactose-regulated genes<sup>19</sup>. To maintain a constant concentration of galactose in the culture medium, cells were grown at low densities so that galactose depletion was negligible (Supplementary Table S2). In Fig. 2a expression histograms are shown for wild-type cells for the two initial conditions and several galactose concentrations. At low galactose concentrations, cells have a basal expression of YFP reflecting low Gal4p activity, whereas at larger galactose

concentrations YFP expression is more than 100-fold higher, reflecting high Gal4p activity. The response to the two different initial conditions depends strongly on the galactose concentration. At low (less than 0.012%) and high (more than 0.35%) galactose concentrations the expression distributions after 27 h do not depend on the history, and typically reach a steady state after 6 h. We classify this behaviour as history independent (absence of memory) because the system approaches the same unique expression distribution when coming from different initial conditions. However, for intermediate galactose concentrations the expression distributions obtained from the two different histories are significantly different and the system displays a memory of the initial galactose consumption state. We classify this behaviour as history dependent (persistent memory) because cells become stably locked into two different expression states for periods much longer than the history-independent system would need to reach steady state. Similar behaviour is obtained when different promoters with Gal4p-binding sites are used (Fig. 3a) to drive YFP expression. In addition, a strong correlation between promoter activities is observed when the activities of two different *GAL* promoters are simultaneously monitored in single cells (Supplementary Fig. S1). This implies that the transcriptional activity of the *GAL1* promoter, and therefore YFP fluorescence, is a faithful reporter for Gal4p activity.

To pinpoint the network interaction responsible for the persistent memory we systematically interrupted the three feedback loops. We found that the positive feedback loop mediated by Gal2p was not

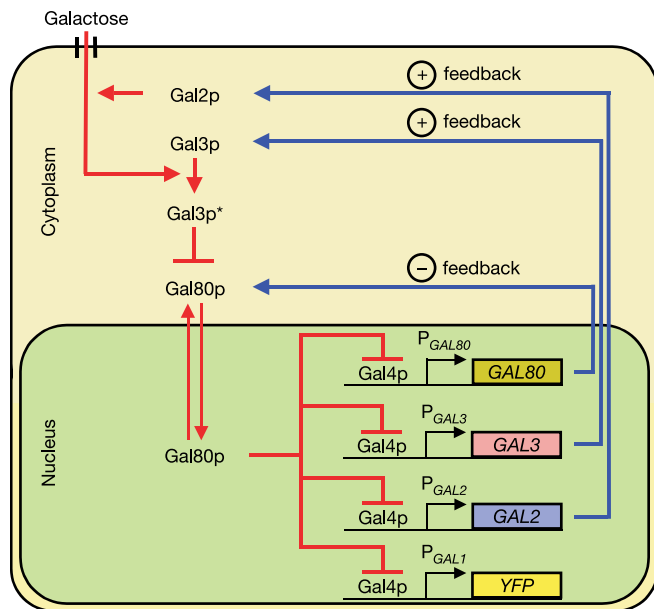


**Figure 1** The galactose signalling pathway. Red arrows denote the four-stage signalling cascade in which the external galactose signal controls the transcriptional activity of the *GAL* genes. The galactose-bound state of Gal3p is denoted by Gal3p\*. Pointed and blunt arrows reflect activation and inhibition, respectively. The double red arrows represent shuttling of Gal80p between the cytoplasm and the nucleus. The blue arrows denote feedback loops established by Gal2p, Gal3p and Gal80p.

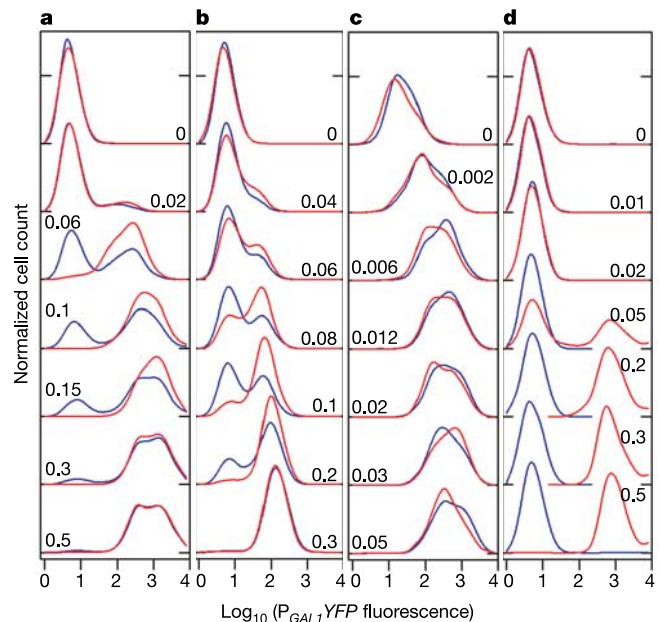


**Figure 2** History-dependent experiments reveal the regulatory interaction necessary for persistent memory. Expression distributions were obtained from at least 10,000 cells and are plotted as a function of  $\log_{10}(\text{YFP fluorescence})$ . Day-to-day variation in the expression histograms is typically less than 5%. Blue and red distributions denote cells that were initially grown for 12 h without galactose (but with 2% raffinose) and with 2% galactose (and 2% raffinose), respectively. After this initial incubation cells were grown for a further 27 h in various concentrations of galactose as specified. **a**, Wild-type strain MA0207. **b**,  $\Delta gal2$  strain MA0215. The intensity of the high state is about 50-fold smaller than wild type. **c**, *GAL3* loop knockout (MA0182). A doxycycline concentration of  $0.05 \mu\text{g ml}^{-1}$  was used. For this concentration the Gal3p expression corresponds to 80% of the Gal3p level observed in a wild-type strain induced with 0.5% galactose (Supplementary Fig. S2). **d**, *GAL80* loop knockout (MA0188). A doxycycline concentration of  $0.05 \mu\text{g ml}^{-1}$  was used. For this concentration the Gal80p expression is very similar to the Gal80p level observed in a wild-type strain induced with 0.5% galactose (Supplementary Fig. S4).

necessary for memory storage (Fig. 2b). *gal2Δ* cells still display history-dependent behaviour, although the expression difference between the two states is reduced. In this case galactose is taken up by non-essential sugar transporters<sup>20</sup>. The non-essential nature of this feedback loop for memory storage contrasts with prokaryotic metabolic networks, in which positive feedback through sugar transporters often defines the dynamics of the system<sup>21</sup>.

To explore the role of the feedback loops through *GAL3* and *GAL80* we constructed loop knockouts in which the feedback loop was interrupted by replacement of the endogenous, Gal4p-dependent, promoter by an externally inducible, Gal4p-independent,  $P_{TET}$  promoter. The capacity of storing the initial galactose consumption state was abolished by disrupting the *GAL3* loop. Irrespective of initial conditions, the cell population approached the same unique distribution (Fig. 2c). The mean expression level increased gradually with increasing galactose concentration, in contrast to the discrete transition observed for the wild-type and *gal2Δ* cells (Fig. 2a, b). This behaviour was observed for the entire *GAL3* expression range examined (from 5% to 300% with respect to wild-type Gal3p levels; Supplementary Fig. S2) and shows that feedback through Gal3p is necessary for memorizing the initial metabolic state in the wild-type network. A slow response of *GAL* genes has been observed in strains lacking a functional *GAL3* gene, several days after induction with galactose<sup>22,23</sup>. The effect of this long-term adaptation depends strongly on which medium or carbon source is used. In our medium, with raffinose always present as a carbon source, long-term adaptation is not observed within 120 h after the addition of galactose to the medium and is therefore not relevant for the memory experiments (Supplementary Fig. S3).

When Gal80p was expressed constitutively at concentrations comparable to those in the wild type, the range of galactose concentration over which this system displayed persistent memory was significantly widened in comparison with wild-type cells (Fig. 2d). This is consistent with the earlier observation that the positive feedback through Gal3p is necessary for memory storage. In wild-type cells the negative feedback through Gal80p effectively weakens the effect of the positive feedback through Gal3p and therefore decreases the persistent memory region in comparison with the *GAL80* loop knockout in which the negative feedback is abolished. For a high concentration of galactose (more than 0.1%) the expression distributions after 27 h are indistinguishable from the initial conditions, showing extreme persistence of the initial expression states. For example, cells initially grown in the absence of galactose still exhibited the same low Gal4p activity level even after 27 h of growth in 0.5% galactose. At this galactose concentration wild-type cells would display maximum Gal4p activity (Fig. 2a). In this regime the initial condition determines the future expression state, not the current concentration of galactose in the medium.

This system was systematically explored over a broad range of *GAL80* expression (Fig. 3b, Supplementary Fig. S4). In a large part of parameter space (galactose versus *GAL80* expression) the system displays persistent memory bordered by regions in which system memory is absent. In the latter case the system either approaches a state of low Gal4p activity (OFF) or high Gal4p activity (ON) independently of the history. Interestingly, at lower *GAL80* expression level a small region in parameter space was identified in which system behaviour displayed destabilized memory. In this region the expression distribution displayed two distinct peaks; however, the system response was not history dependent. We proposed that although the system has two stable states, fluctuations in the gene expression of key regulators drive random transitions between the two states, resulting in a destabilization of the memory. Indeed, a significant cell-to-cell variation of gene expression levels was observed for several promoters in budding yeast<sup>24,25</sup>.

To reveal the effect of these fluctuations on the memory, the stability of the expression states was quantified by using the concept

of energy landscapes<sup>26–28</sup>. The first-order differential equation describing the time evolution of the Gal3p concentration is analogous to the equation of motion of an overdamped particle in an energy landscape, where the particle position is analogous to the concentration of Gal3p. This analogy provides an intuitive representation for the stability of cellular expression states because minima in the energy landscape correspond to stable states that are separated by an energy barrier (Fig. 3c). Fluctuations in gene expression are naturally introduced by analogy with the temperature experienced by the particle in the energy landscape. A particle trapped in an energy well at zero temperature will never escape; however, at elevated temperatures the particle will undergo thermally activated transitions across the barrier. In this case the escape rate is proportional to  $\exp(-\Delta U/k_B T)$ , where  $\Delta U$  represents the energy barrier,  $k_B$  the Boltzmann constant and  $T$  the absolute temperature<sup>29</sup>. The larger the energy barrier, the more efficiently the fluctuations are trapped in the vicinity of the stable states. The *GAL* system is characterized by two energy barriers: the barrier  $\Delta U_{OFF \rightarrow ON}$  that an OFF cell has to overcome to switch ON, and the barrier  $\Delta U_{ON \rightarrow OFF}$  for the opposite transition. The barrier height

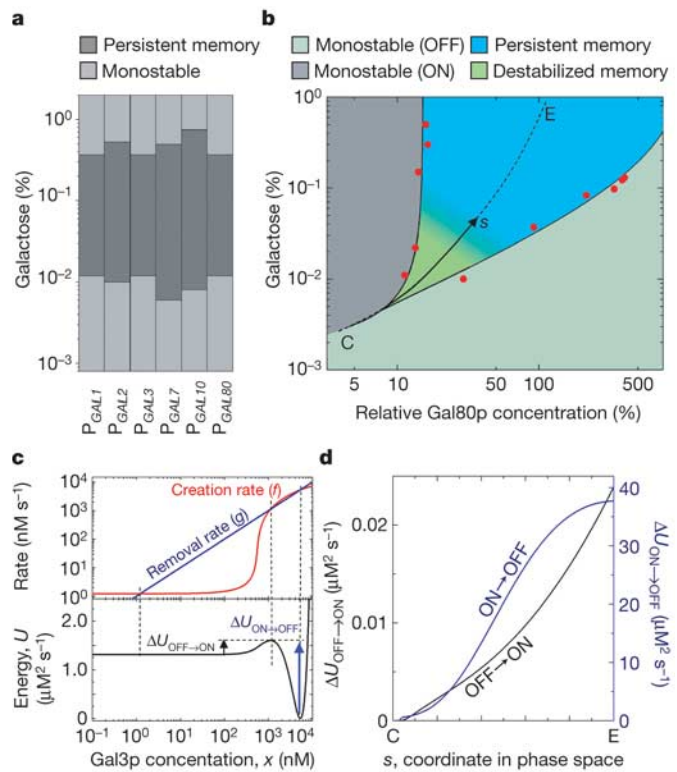


**Figure 3** Stability analysis of the *GAL* network. **a**, The range over which the system displays persistent memory is similar for different strains (columns from left to right: MA0207, MA0208, MA0231, MA0212, MA0213, MA0242) in which the reporter gene is driven by different *GAL* promoters. **b**, System behaviour as a function of the control parameters: the external galactose concentration and the intracellular Gal80p concentration. *GAL80* expression is controlled by a doxycycline-inducible promoter (MA0188) and is measured relative to wild-type Gal80p expression (induced by 0.5% galactose; Supplementary Fig. S4). Red circles indicate experimentally determined boundaries between different system behaviours, and the black solid lines represent the theoretical prediction based on the regulatory network depicted in Fig. 1. The critical point is defined as C. The coordinate  $s$  defined on the path from C to the endpoint E is used in **d** to demonstrate the concept of energy barriers. **c**, The energy landscape was calculated by integrating the difference between the creation  $f(x)$  and destruction rates  $g(x)$  of Gal3p with respect to the Gal3p concentration denoted by  $x$ . The corresponding equation is  $U(x) = -\int_0^x [f(x') - g(x')] dx'$ . **d**, Magnitude of the energy barriers as a function of the coordinate  $s$  from C to E as defined in **b**.

depends strongly on the system parameters. The barriers are high in the ‘persistent memory’ region and vanish as the critical point C is approached at lower *GAL80* expression level (Fig. 3b, d).

These predictions were verified by measuring the switching rates between the two states (Fig. 4). For this purpose we monitored the time evolution of the expression distribution as the system approached steady state. An example of a bimodal distribution is shown in Fig. 4a (top graph) obtained from the *GAL80* loop knockout operating in the ‘destabilized memory’ region (Fig. 3b): some cells had high Gal4p activity but other cells had 100-fold lower Gal4p activity. From this mixed population, two subpopulations were sorted representing the two extremes of this distribution (Fig. 4a,  $t = 0$ ). Subsequently, these two subpopulations were grown separately in the same medium as before sorting. The example in Fig. 4a shows that both subpopulations relaxed back to the same bimodal distribution. These experiments therefore rule out static disorder and indicate that cells switch back and forth between expression states. The switching rates strongly depended on the Gal80p level and the galactose concentration (Fig. 4b). When the system operated in the ‘destabilized memory’ region close to the critical point C (Fig. 3b) the system approached steady state in about 10 h (Fig. 4b, circles). However, if the system operated closer

to the boundary between the destabilized and persistent memory regions this process took much longer (Fig. 4b, triangles). At sufficiently high barriers, cells were almost irreversibly locked in one of the cellular states.

Figure 4c shows the experimental escape rates as a function of the calculated energy barrier. Escape rates decreased precipitously as the height of the energy barrier increases, a correlation typical of noise-induced transitions bounded by energy barriers. For the same barrier height, escape rates from the ON state were larger than escape rates from the OFF state. Indeed, the fluctuations in *GAL3* expression were larger in the ON state than in the OFF state (Supplementary Fig. S5). However, given the complexity of this network and the presence of multiple noise sources<sup>24,25</sup>, it is unlikely that *GAL3* expression fluctuations can solely account for this difference in switching rates.

Next we explored whether cellular memory could affect the growth rate of a population. Increased growth rate of the ON cells relative to the OFF cells was observed when the cells were grown in medium in which galactose was the predominant carbon source (Supplementary Fig. S6). Because the fraction of ON cells in a population is strongly dependent on cellular memory, this indicates that memory might be a significant concept in understanding the fitness of a population in habitats in which carbon sources are fluctuating.

The galactose signalling pathway of budding yeast has the potential for reliably storing information on previous galactose exposures for hundreds of generations. A core positive feedback loop through *GAL3* is necessary for this cellular memory, whereas a negative feedback loop through *GAL80* competes with the positive *GAL3* loop and reduces the potential for memory storage. Consistently, when the negative feedback loop is opened and Gal80p levels are controlled constitutively, the memory persistence can be tuned from hours to months. A quantitative understanding of cellular differentiation would require a similar system-level approach to the one that we employed for the galactose signalling pathway. Systematically opening the underlying feedback loops complemented by stochastic and stability analyses provides a quantitative tool for identifying network architectures responsible for the stability of differentiated cellular states. □

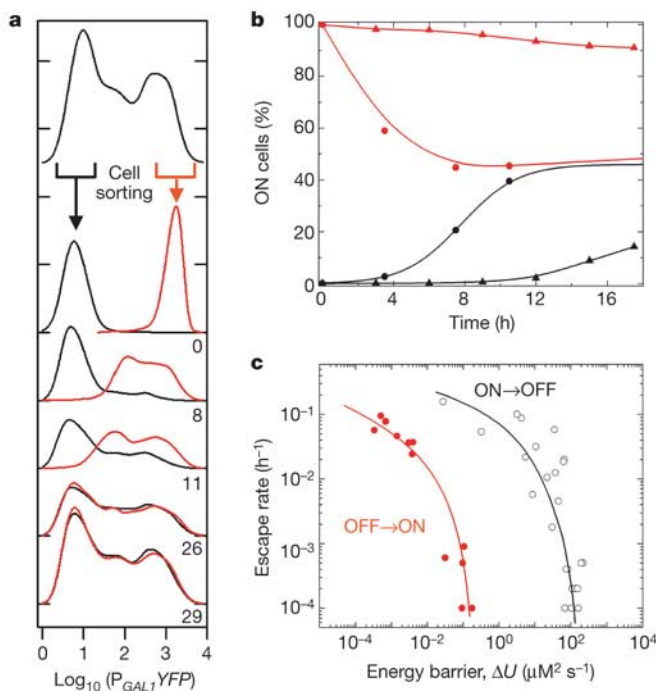


**Figure 4** Stochastic switching dynamics between two stable expression states (strain MA0188). **a**, An initially bimodal population (0% galactose and  $0 \mu\text{g ml}^{-1}$  doxycycline, 27 h of growth after raffinose history) was sorted by fluorescent activated cell sorting into cells expressing low and high levels of YFP. At different times, indicated in hours after sorting, expression distributions were measured. **b**, The fraction of ON cells as a function of time after sorting in the absence of doxycycline and galactose (filled circles) and in the presence of  $0.01 \mu\text{g ml}^{-1}$  doxycycline and  $0.04\%$  galactose (filled triangles). Black and red solid lines (guides to the eye) reflect the sorted population that was initially fully OFF and ON, respectively. The standard error on the fractions is smaller than 5% as determined by reproducing a representative histogram 10 times. **c**, Experimentally measured escape rates (Supplementary Information) as a function of the calculated energy barriers. Black lines and symbols indicate experimentally determined escape rates from the ON state; red lines and symbols denote escape rates from the OFF state. Energy barriers were calculated with experimentally determined parameters obtained from fitting the experimentally determined boundaries (Fig. 3b, red circles) to the network model (Fig. 3b, solid black lines; Supplementary Information). The solid lines are guides to the eye.

## Methods

### Plasmid and strain constructions

*KpnI*-promoter-*BamHI*, *BamHI*-YFP-*EcoRI* fragments were cloned into pRS402 backbone upstream of *CYC1* transcriptional terminator (for *P<sub>GAL4</sub>* promoter, *BgIII* was used instead of *BamHI*). The *P<sub>GAL1</sub>*, *P<sub>GAL2</sub>*, *P<sub>GAL3</sub>*, *P<sub>GAL4</sub>*, *P<sub>GAL6</sub>*, *P<sub>GAL7</sub>*, *P<sub>GAL10</sub>*, *P<sub>GAL80</sub>* and *P<sub>MYO2</sub>* promoter sequences correspond to 669, 960, 830, 633, 590, 724, 667, 632 and 677 base-pair regions upstream of the start codon of the respective genes. The *GAL3* and *GAL80* genes were cloned downstream of *KpnI*-*P<sub>TET2</sub>*-*BamHI* as *BamHI*-*EcoRI* fragments into pRS306. *P<sub>GAL3</sub>*-*GAL3*, *P<sub>GAL80</sub>*-*GAL80*, *P<sub>TET2</sub>*-*GAL3* and *P<sub>TET2</sub>*-*GAL80* lacking the stop codon were cloned upstream of *BamHI*-*CFP*-*EcoRI* as *KpnI*-*BamHI* fragments in pRS306. All strains were derived from W303. Polymerase chain reaction and Southern blotting were used to verify the integrations. Complete descriptions of the strains used in this study can be found in Supplementary Information.

### Growth conditions and media

Cultures were grown in synthetic dropout media with the appropriate amino-acid supplement and 2% raffinose as a carbon source. Media used for ‘galactose history’ experiments were supplemented with 2% galactose, whereas media for ‘raffinose history’ experiments contained raffinose as the sole carbon source. Cells grown overnight were diluted to a  $D_{600}$  value such that after 27 h of growth the galactose concentration in the medium would not change by more than 10% (Supplementary Information). Cells were grown at  $30^\circ\text{C}$ . After the induction period of 27 h, the expression distributions were determined by flow cytometer (FACScan; Becton Dickinson). For cell sorting, the bimodally distributed cells were sorted into OFF and ON cells as indicated in Fig. 4a.

### Gal3p and Gal80p levels in inducible strains relative to wild-type levels

To determine how Gal3p and Gal80p levels in strains MA0182 and MA0188, respectively, compared with native levels of Gal3p and Gal80p in wild-type cells, strains were constructed in which the carboxy terminus of Gal3p and Gal80p was fused to CFP. The levels of doxycycline-induced *GAL3* and *GAL80* expression relative to the wild-type expression were determined by fluorescence microscopy. We found that the addition of  $0.07$  and  $0.05 \mu\text{g ml}^{-1}$  doxycycline resulted in the expression of wild-type levels (wild-type

cells fully induced with 0.5% galactose) of Gal3p and Gal80p, respectively (Supplementary Figs S2 and S4).

## Determination of galactose consumption rate

To determine the galactose consumption rate, aliquots from cultures were filtered and the galactose concentration of the cell-free medium was analysed as follows.  $\beta$ -Galactose dehydrogenase was used to oxidize galactose in the presence of 2.5 mM NAD<sup>+</sup> dissolved in a buffer containing 50 mM imidazole and 5 mM MgCl<sub>2</sub> pH 7.0 (ref. 30). Conversion of NAD<sup>+</sup> into NADH was followed spectrophotometrically at 340 nm.

Received 2 February; accepted 9 March 2005; doi:10.1038/nature03524.

1. Freeman, M. Feedback control of intercellular signalling in development. *Nature* **408**, 313–319 (2000).
2. Davidson, E. H. *et al.* A genomic regulatory network for development. *Science* **295**, 1669–1678 (2002).
3. Xie, H., Ye, M., Feng, R. & Graf, T. Stepwise reprogramming of B cells into macrophages. *Cell* **117**, 663–676 (2004).
4. Xiong, W. & Ferrell, J. E. Jr. A positive-feedback-based bistable ‘memory module’ that governs a cell fate decision. *Nature* **426**, 460–465 (2003).
5. Shykind, B. M. *et al.* Gene switching and the stability of odorant receptor gene choice. *Cell* **117**, 801–815 (2004).
6. Markevich, N. I., Hoek, J. B. & Kholodenko, B. N. Signalling switches and bistability arising from multisite phosphorylation in protein kinase cascades. *J. Cell Biol.* **164**, 353–359 (2004).
7. Gardner, T. S., Cantor, C. R. & Collins, J. J. Construction of a genetic toggle switch in *Escherichia coli*. *Nature* **403**, 339–342 (2000).
8. Becskei, A., Seraphin, B. & Serrano, L. Positive feedback in eukaryotic gene networks: cell differentiation by graded to binary response conversion. *EMBO J.* **20**, 2528–2535 (2001).
9. Atkinson, M. R., Savageau, M. A., Myers, J. T. & Ninfa, A. J. Development of genetic circuitry exhibiting toggle switch or oscillatory behavior in *Escherichia coli*. *Cell* **113**, 597–607 (2003).
10. Isaacs, F. J., Hasty, J., Cantor, C. R. & Collins, J. J. Prediction and measurement of an autoregulatory genetic module. *Proc. Natl Acad. Sci. USA* **100**, 7714–7719 (2003).
11. Angeli, D., Ferrell, J. E. Jr. & Sontag, E. D. Detection of multistability, bifurcations, and hysteresis in a large class of biological positive-feedback systems. *Proc. Natl Acad. Sci. USA* **101**, 1822–1827 (2004).
12. Lai, K., Robertson, M. J. & Schaffer, D. V. The sonic hedgehog signaling system as a bistable genetic switch. *Biophys. J.* **86**, 2748–2757 (2004).
13. Biggar, S. R. & Crabtree, G. R. Cell signaling can direct either binary or graded transcriptional responses. *EMBO J.* **20**, 3167–3176 (2001).
14. Ideker, T. *et al.* Integrated genomic and proteomic analyses of a systematically perturbed metabolic network. *Science* **292**, 929–934 (2001).
15. Suzuki-Fujimoto, T. *et al.* Analysis of the galactose signal transduction pathway in *Saccharomyces cerevisiae*: interaction between Gal3p and Gal80p. *Mol. Cell. Biol.* **16**, 2504–2508 (1996).
16. Timson, D. J., Ross, H. C. & Reece, R. J. Gal3p and Gal1p interact with the transcriptional repressor Gal80p to form a complex of 1:1 stoichiometry. *Biochem. J.* **363**, 515–520 (2002).
17. Peng, G. & Hopper, J. E. Gene activation by interaction of an inhibitor with a cytoplasmic signaling protein. *Proc. Natl Acad. Sci. USA* **99**, 8548–8553 (2002).
18. Mizutani, A. & Tanaka, M. Regions of GAL4 critical for binding to a promoter *in vivo* revealed by a visual DNA-binding analysis. *EMBO J.* **22**, 2178–2187 (2003).
19. Johnston, M., Flick, J. S. & Pexton, T. Multiple mechanisms provide rapid and stringent glucose repression of GAL gene expression in *Saccharomyces cerevisiae*. *Mol. Cell. Biol.* **14**, 3834–3841 (1994).
20. Wiczorke, R. *et al.* Concurrent knock-out of at least 20 transporter genes is required to block uptake of hexoses in *Saccharomyces cerevisiae*. *FEBS Lett.* **464**, 123–128 (1999).
21. Ozbudak, E. M., Thattai, M., Lim, H. N., Shraiman, B. I. & van Oudenaarden, A. Multistability in the lactose utilization network of *Escherichia coli*. *Nature* **427**, 737–740 (2004).
22. Bhat, P. J. & Hopper, J. E. The mechanism of inducer formation in *gal3* mutants of the yeast galactose system is independent of normal galactose metabolism and mitochondrial respiratory function. *Genetics* **128**, 233–239 (1991).
23. Rohde, J. R., Trinh, J. & Sadowski, I. Multiple signals regulate GAL transcription in yeast. *Mol. Cell. Biol.* **20**, 3880–3886 (2000).

24. Blake, W. J., Kaern, M., Cantor, C. R. & Collins, J. J. Noise in eukaryotic gene expression. *Nature* **422**, 633–637 (2003).
25. Raser, J. M. & O’Shea, E. K. Control of stochasticity in eukaryotic gene expression. *Science* **304**, 1811–1814 (2004).
26. Hasty, J., Pradines, J., Dolnik, M. & Collins, J. J. Noise-based switches and amplifiers for gene expression. *Proc. Natl Acad. Sci. USA* **97**, 2075–2080 (2000).
27. Bialek, W. Stability and noise in biochemical switches. *Adv. Neural Info. Process.* **13**, 103–109 (2001).
28. Kepler, T. B. & Elston, T. C. Stochasticity in transcriptional regulation: origins, consequences, and mathematical representations. *Biophys. J.* **81**, 3116–3136 (2001).
29. Kramers, H. A. Brownian motion in a field of force and the diffusion model of chemical reactions. *Physica* **7**, 284–304 (1940).
30. Silje, H. H. *et al.* Effects of different carbon fluxes on G1 phase duration, cyclin expression, and reserve carbohydrate metabolism in *Saccharomyces cerevisiae*. *J. Bacteriol.* **179**, 6560–6565 (1997).

Supplementary Information accompanies the paper on [www.nature.com/nature](http://www.nature.com/nature).

**Acknowledgements** We thank M. Thattai for stimulating discussions and helpful suggestions on measuring the escape rates; J. Pedraza, M. Kardar, O. Ozcan and S. Cabi for useful discussions; B. Kaufmann for help with image analysis; and B. Pando for comments on the manuscript. M.A. acknowledges support by an MIT Presidential Fellowship endowed by Praecis Pharmaceuticals, Inc. A.B. is a Long Term Fellow of the Human Frontiers Science Program. This work was supported by a NSF-CAREER and a NIH grant.

**Competing interests statement** The authors declare that they have no competing financial interests.

**Correspondence** and requests for materials should be addressed to A.v.O. ([avano@mit.edu](mailto:avano@mit.edu)).

---

## corrigendum

---

# Iron and phosphorus co-limit nitrogen fixation in the eastern tropical North Atlantic

**Matthew M. Mills, Celine Ridame, Margaret Davey, Julie La Roche & Richard J. Geider**

*Nature* **429**, 292–294 (2004).

In this Letter to *Nature*, the chlorophyll *a* data presented in Fig. 1d–f and in Table S1 of the Supplementary Information are an order of magnitude too low owing to a calculation mistake. This error does not alter the conclusions of our paper. □